Interaction Dependent Heating and Atom Loss in a Periodically Driven Optical Lattice

Martin Reitter,[1,2] Jakob Näger,[1,2] Karen Wintersperger,[1,2] Christoph Sträter,[3]
Immanuel Bloch,[1,2] André Eckardt,[3] and Ulrich Schneider[4]

[1]*Fakultät für Physik, Ludwig-Maximilians-Universität München, Schellingstraße 4, 80799 Munich, Germany*
[2]*Max-Planck-Institut für Quantenoptik, Hans-Kopfermann-Straße 1, 85748 Garching, Germany*
[3]*Max-Planck-Institut für Physik komplexer Systeme, Nöthnitzer Straße 38, 01387 Dresden, Germany*
[4]*Cavendish Laboratory, University of Cambridge, J. J. Thomson Avenue, Cambridge CB3 0HE, United Kingdom*
(Received 29 June 2017; published 16 November 2017)

Periodic driving of optical lattices has enabled the creation of novel band structures not realizable in static lattice systems, such as topological bands for neutral particles. However, especially driven systems of interacting bosonic particles often suffer from strong heating. We have systematically studied heating in an interacting Bose-Einstein condensate in a driven one-dimensional optical lattice. We find interaction dependent heating rates that depend on both the scattering length and the driving strength and identify the underlying resonant intra- and interband scattering processes. By comparing the experimental data and theory, we find that, for driving frequencies well above the trap depth, the heating rate is dramatically reduced by the fact that resonantly scattered atoms leave the trap before dissipating their energy into the system. This mechanism of Floquet evaporative cooling offers a powerful strategy to minimize heating in Floquet engineered quantum gases.

Introduction.—Floquet engineering, the coherent control of quantum systems by means of time-periodic driving, enables the realization of novel band structures and many-body phases beyond what is possible in static systems [1–12]. It has become an important tool for studies of quantum gases [13], where it, e.g., enables the breaking of time-reversal symmetry and thereby the realization of topological bands even for charge-neutral particles [5, 10–12]. In the form of infrared laser pulses, time-periodic driving can give rise to novel effects in traditional condensed matter systems, such as graphenelike systems [14–16] or high-temperature superconductors [17–19]. It also lies at the heart of the recently realized discrete time crystals [20–25].

Despite those recent accomplishments, successfully combining periodic driving with interactions remains a major experimental challenge: In a driven system, energy is not conserved, as the system can absorb or emit energy from or into the drive. Therefore, for any fully ergodic driven system, there can only be one steady state, namely, the fully mixed density matrix corresponding to an infinite temperature state [26–39]. While this scenario could be avoided by using nonergodic systems, such as, e.g., many-body localized states [40], their use cannot solve the problem, in general, as many interesting phases, such as fractional quantum Hall states, are typically ergodic. Therefore, one has to find setups and parameter regimes that allow experimental studies of novel, driven phases on intermediate time scales before the unavoidable heating dominates.

In this work, we experimentally study loss rates of condensed atoms in a driven optical lattice as a function of both the driving and interaction strength and can thereby distinguish single-particle from interaction effects. Single-particle heating occurs via discrete single- or multiphoton interband resonances [41] that can easily be avoided. This is in contrast to two-particle processes, which in one- or two-dimensional lattices are always resonant, as collisions can convert arbitrary energies into transverse excitations [32,34,35]. This is in stark contrast to three-dimensional lattices, where these processes can be suppressed [28,32,34]. We focus on the two experimentally most relevant driving regimes: For low shaking frequencies ω much smaller than the resonance frequency to the first excited band but above the bandwidth of the lowest band, the tunneling matrix element of the lowest band is effectively renormalized by a Bessel function (corresponding to dynamic localization [42,43]). At the same time, multi-photon resonances are weak, as they require many photons. This regime is typically employed for engineering artificial gauge fields [3,5,12]. The second regime lies between the two lowest single-photon single-particle resonances. Here, the dispersion relation can acquire two separate minima that can be exploited to study the formation of symmetry-broken domains [4,6]. We find that for large driving frequencies heating is strongly reduced by the fact that scattered particles with energy $\sim\hbar\omega$ typically leave the trap before dissipating the absorbed energy into the system.

Experimental setup.—We load an almost pure Bose-Einstein condensate (BEC) of about 4×10^5 [39]K atoms into the lowest band of a one-dimensional lattice with lattice constant $a = 425$ nm, which is created by interfering two blue-detuned laser beams with a wavelength of
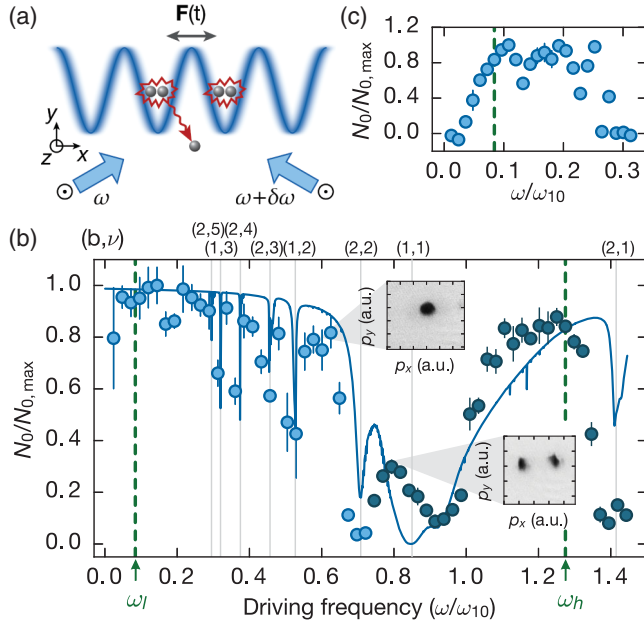
FIG. 1. Schematic of the experiment and frequency scan. (a) Two lattice beams with a linear out-of-plane polarization intersect at an angle of 120° to form a one-dimensional lattice of "pancakes." By periodically modulating the frequency of one of the lattice beams, we can shake the lattice, i.e., modulate its position. (b) Normalized atom number after modulating for 50 (for $\omega/\omega_{10} > 0.7$) or 100 ms (for $\omega/\omega_{10} < 0.7$) with variable frequency at a driving strength of $\alpha \simeq 0.9$. Error bars indicate the standard error of the mean from four measurements per data point. The solid blue line shows the theoretically expected single-particle excitations to higher bands. Thin lines mark the resonance positions of single- and multiphoton transitions to higher bands labeled by (b, ν). In the frequency region from roughly $0.7\omega_{10}$ to $1.1\omega_{10}$, we observe a splitting of the BEC due to two degenerate minima in the lowest dressed band, which is included in the theory curve. The insets show raw quasimomentum images of the BEC. (c) Enlargement into the regime of small shaking frequencies with $\alpha = 2.2$ and 200 ms shaking duration.

$\lambda = 736.8$ nm at an angle of $\theta = 120°$; see Fig. 1(a). Then, we shake the lattice position by periodically modulating the frequency of one of the two laser beams. The atoms feel a periodic inertial force in the frame comoving with the lattice, which is given by $F_x(t) = -(K/a)\cos(\omega t)$, where we have introduced the driving amplitude K. In order to avoid strong, non-adiabatic excitations to higher bands during the switch on of the modulation, we continuously ramp the driving amplitude in 10 ms to its desired value. After a variable shaking duration, we determine the heating and losses induced by the drive by measuring the remaining atom number in the BEC. To this end, we abruptly stop the drive after an integer number of shaking cycles, immediately followed by band mapping in the static lattice and 15 ms of time-of-flight (TOF). This TOF is long enough to dilute any thermal background such that we can

reliably determine the remaining number of condensed atoms. For all measurements, we use a lattice depth of $V_0 = 11.0(3)E_r$, where $E_r = h^2/(8Ma^2) \approx h \times 7.1$ kHz is the effective recoil energy of this lattice with M being the mass of ^{39}K. In this static lattice, the first interband excitation at zero momentum appears at a frequency of $\omega_{10} = 2\pi \times 41.6(5)$ kHz.

Frequency scan.—Single-particle transitions occur only at specific resonances where the shaking frequency ω fulfills a multiphoton resonance condition $\nu\hbar\omega \simeq \Delta_{b0}(q)$, with ν being an integer and $\Delta_{b0}(q)$ denoting the separation of the lowest band to the bth excited band at a given quasimomentum q. To ensure that we avoid these resonances, we measure the remaining BEC atom number after shaking with variable frequency at a dimensionless driving strength $\alpha \equiv K/(\hbar\omega)$ and scattering length $a_s = 60a_0$, with a_0 being Bohr's radius, using a Feshbach resonance at 400 G [44]; see Fig. 1. The solid blue line shows the result of a numerical single-particle simulation assuming a Gaussian width of the BEC in momentum space of $\Delta q = 0.2\pi/a$ (for the method, see [41,45]). While the resonances at large frequencies are clearly visible, multiphoton resonances at small driving frequencies are highly suppressed. For our subsequent lifetime measurements, we choose $\omega_l = 0.084\omega_{10}$ and $\omega_h = 1.27\omega_{10}$ (green dashed lines) as low and high frequency, far away from all single-particle resonances.

Experimental loss rates.—The total loss rate of condensate atoms in our system is given by summing over background losses in the static system, characterized by a lifetime τ, and heating and losses induced by lattice shaking. We assume that all losses happen on a sufficiently slow time scale such that the system heats up but stays in global thermal equilibrium and describe the condensed part using the Thomas-Fermi approximation. We have verified independently that the cloud size indeed shrinks according to the decreasing number of condensed atoms N_0 [45]. Within this approximation, the driving-induced loss rate of condensate atoms due to two-particle collisions takes the form $-\kappa N_0^{7/5}$ [45]. Including the background losses $-N_0/\tau$ of the static system, we obtain

$$N_0(t) = N_0(0)e^{-t/\tau}[1 + N_0(0)^{2/5}\kappa\tau(1 - e^{-2t/(5\tau)})]^{-5/2}. \tag{1}$$

We measure τ independently for each scattering length in the static lattice. In order to form a more intuitive quantity, we define a scaled loss rate $\tilde{\kappa} = \kappa N_0(0)^{2/5}$ such that the initial driving-induced losses scale as $\propto \tilde{\kappa}N_0(0)$. As shown in Fig. 2, both stronger interactions and larger driving strengths lead to dramatically higher loss rates for the BEC.

Theoretical description.—In order to identify and estimate the dominant heating channels associated with two-particle scattering, we start by describing a homogeneous system in the Floquet space of time-periodic states, where an integer Fourier index m describes the change in the "photon" number relative to a large classical background;
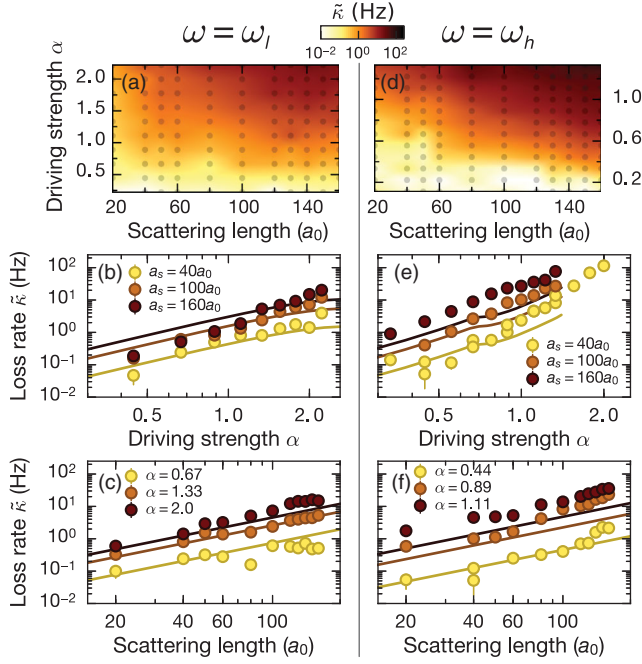
FIG. 2. Loss rates in the presence of periodic driving. (a),
(d) Effective loss rates for different driving amplitudes and
scattering lengths. Each dot corresponds to a single lifetime
measurement. The shaking frequency is (a)–(c) $\omega = \omega_l$ and (d)–
(f) $\omega = \omega_h$. (b),(e) Crosscuts at fixed scattering lengths. The solid
lines correspond to the theoretically predicted scattering rates,
and error bars indicate fit uncertainties. (c),(f) Corresponding
crosscuts at fixed driving strengths. Theory lines in (b),(c) assume
$f\beta\hbar\omega = 10$ to account for the thermalization of scattered atoms
(see the text).

i.e., $-m$ counts the number of absorbed photons. In this
dressed-atom-like picture, the dynamics is generated by the
quasienergy operator Q. Within the subspace of a given
relative photon number m, it acts like $Q_{m,m} = H^{(0)} + m\hbar\omega$,
whereas the coupling between subspaces m' and m corre-
sponds to an $(m - m')$ photon process which is captured
by $Q_{m',m} = H^{(m'-m)}$. Here $H^{(\nu)} = (1/T)\int_0^T dt\, e^{i\nu\omega t}H(t)$
denotes the νth Fourier component of the time-dependent
Hamiltonian $H(t)$. The time-averaged Hamiltonian $H^{(0)}$
describes a dispersion relation $\varepsilon_b(k_x) + E_\perp(k_y, k_z)$, with
effective band structure $\varepsilon_b(k_x)$ and transverse kinetic
energy $E_\perp = \hbar^2(k_y^2 + k_z^2)/(2M)$, as well as interactions.

In Fig. 3, we sketch the lowest two bands $b = 0, 1$ for the
relative photon numbers $m = 0, -1$ (solid and dashed lines,
respectively), given by $\varepsilon_b(k_x) + m\hbar\omega$. The diagrams depict
three examples of relevant scattering channels, where two
particles (small spheres) are excited out of the condensate
into the states $|b, \boldsymbol{k}\rangle$ and $|b', -\boldsymbol{k}\rangle$ absorbing $\nu = m - m'$
photons, as indicated by the number of particles transferred
to the dashed bands [$\nu = 1$ in Fig. 3(b) and $\nu = 2$ in
Figs. 3(a) and 3(c)]. The resonance condition for two-
particle excitations can be written as

$$\varepsilon_b(k_x) + \varepsilon_{b'}(-k_x) - \nu\hbar\omega - 2\varepsilon_0(0) = -2E_\perp \leq 0. \quad (2)$$
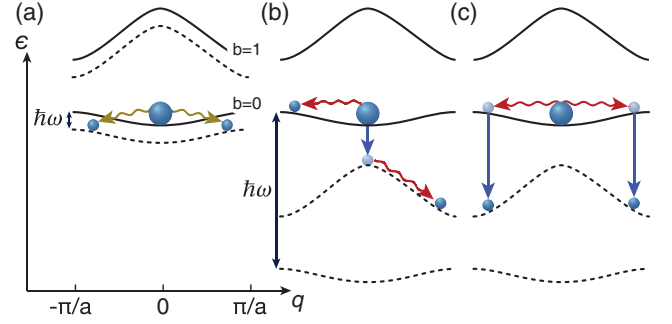
FIG. 3. Examples of two-particle scattering channels. The
lowest two bands of a schematic lattice dispersion are sketched
by solid lines, and Floquet modes shifted by $-\hbar\omega(m = -1)$ are
depicted by dashed lines. The condensate is represented by a
large sphere, and scattered particles by small spheres. The pair of
yellow wiggly arrows in (a) denotes a two-photon scattering
process, where the atoms absorb two photons, while the red
wiggly lines in (b),(c) denote a zero-photon (ordinary) collision
between two atoms, and blue arrows describe single-photon
interband transitions. (a) When the driving frequency is much
smaller than the band gap, the dominant loss process are two-
photon intraband collisions. (b),(c) For driving frequencies larger
than the band gap, the leading (subleading) excitation channels
combine one (two) single-photon interband transitions with zero-
photon collisions. Note that only one photon number m is
associated with the whole system and not one per particle as
suggested, for simplicity, in the diagrams.

Here, we have separated the transverse kinetic energy
$2E_\perp = E_\perp(k_y, k_z) + E_\perp(-k_y, -k_z)$ created in the scatter-
ing process on one side of the equation. As there is no
lattice potential along these directions, the transverse
kinetic energy can take arbitrary non-negative values. As
a consequence, in Fig. 3 all states with a total energy below
the original BEC are accessible.

For the smaller driving frequency ω_l, the tunneling in the
lowest band is modified by a Bessel function $J_{\mathrm{eff}} =
\mathcal{J}_0(\alpha)J_0$ [45,52], where $\mathcal{J}_\nu(\alpha)$ is a Bessel function and
J_0 the tunneling matrix element of band $b = 0$. In this
regime, scattering particles to an excited band would
require absorbing a large number of photons. Therefore,
the dominant heating channel is *intraband* scattering with
small ν. Processes with odd ν are forbidden by symmetry
for a condensate with zero momentum and acquire finite
values only due to the momentum spread of the condensate
[45]. For a ν-photon scattering process, the matrix element
scales like $\sim\hbar^2 a_s n_0 J_0 \mathcal{J}_\nu(\alpha)/(\nu\hbar\omega M)$ [45], with a prefac-
tor that for odd ν is about 5 times smaller than for even ν at
the measured momentum spread of $0.2\pi/a$ and where n_0 is
the condensate density.

For the larger driving frequency ω_h, *interband* scattering
dominates. In this regime, single-photon single-particle
interband coupling is strong (with matrix elements $\sim\alpha E_r$
[45]) but off resonant. This leads to a perturbative admixture
of states from the first excited band ($b = 1$) with $m = -1$ to
the lowest band ($b = 0$) with $m = 0$ and vice versa. As a

result of this coupling, already ordinary zero-photon collisions, which are stronger than ν-photon scattering processes, give rise to excitations by scattering atoms between these dressed bands. Another consequence of this admixture of the highly dispersive first excited band to the rather narrow lowest band is the formation of a double-well structure within the lowest band for sufficiently large driving strengths α [4,6,45]. As a result, the condensate reforms at the new minima of the dispersion at finite quasimomenta; see the insets in Fig. 1(b). We compute the matrix elements for resonant interband excitations using degenerate perturbation theory. In leading order, we encounter three different single-photon ($\nu = 1$) processes, such as the one depicted in Fig. 3(b), involving a single-particle single-photon interband transition and a zero-photon two-particle scattering event. Their matrix elements scale like $\sim \hbar^2 a_s n_0 E_r \alpha / (\hbar \omega M)$. The leading correction stems from two-photon ($\nu = 2$) processes, an example of which is shown in Fig. 3(c), giving rise to matrix elements that are a factor of $\alpha E_r / (\hbar \omega)$ smaller [45].

Applying Fermi's golden rule and integrating over the time-dependent Thomas-Fermi profile in a local density approximation, we derive the rates Γ_ν of atoms scattered out of the condensate via ν-photon processes [45] and find that they are proportional to $(a_s N_0)^{7/5}$. For the lower driving frequency ω_l, the scattered particles will not have enough energy to leave the trap and will dissipate their entire energy into the system via ordinary (zero-photon) collisions. This excites additional atoms out of the condensate, leading to a decay rate for condensed atoms $\dot{N}_0 = -f\beta\hbar\omega \sum_\nu \nu\Gamma_\nu / 2$ with inverse temperature β and a numerical factor $f \sim O(1)$ that depends on the details of the system [45]. Because of the finite momentum of these newly created thermal atoms, $\nu = 1$ scattering now becomes dominant, and they will absorb photons at an even faster rate than condensed atoms. In a truly closed system, this form of heating would scale linearly with the photon energy $\hbar\omega$. Because of the finite trap depth, however, the system is effectively open, and, for the higher driving frequency ω_h, scattered particles typically have sufficient energy to quickly leave the trap without dissipating the absorbed energy. In this regime, we expect $\dot{N}_0 = -\sum_\nu \Gamma_\nu$.

Comparison between theory and experiment.—Because of the thermalization of the absorbed photon energies described above, the measured loss rates of condensed atoms at low driving frequency ω_l will be larger than the total scattering rate $\sum_\nu \Gamma_\nu$ [Figs. 2(a)–2(c)]. We observe a factor of $f\beta\hbar\omega \approx 10$, which provides a lower bound for the temperature of the condensate. Assuming for simplicity an ideal homogeneous gas results in a realistic lower bound of 15 nK. While typical temperatures of the BEC will likely be higher [45], the differences are most likely due to resonant scattering of thermal atoms, which is not included in the theory. In contrast, for a driving frequency of ω_h, shown in Figs. 2(d)–2(f), the loss rate of condensed atoms coincides

with the total scattering rate, since the absorbed photon energy is carried away with the scattered particles leaving the trap. This highlights the advantage of working at larger driving frequencies.

Figures 2(c) and 2(f) show a rather good general agreement with the expected scaling with the scattering length of $\dot{N}_0 \propto a_s^{7/5}$, demonstrating that the dominant loss mechanisms are indeed interaction driven and that the Thomas-Fermi local-density approximation is consistent with our data. While the data at large driving frequency ω_h follow the theory rather well for not too strong interactions and driving, we observe increasing discrepancies for both larger scattering lengths and larger driving strengths. When the mean free path of excited atoms ($\propto 1/a_s^2$) becomes on the order of the size of the BEC, excited atoms will undergo additional collisions while leaving the cloud, thereby giving rise to an additional loss of condensate atoms similarly to the low-frequency case [45]. This is most clearly visible when plotting the data vs scattering length; see Fig. 2(f), where for weak driving a discrepancy to the $a_s^{7/5}$ scaling can be observed for scattering lengths larger than $\simeq 100a_0$. For higher driving strengths, we expect the onset of additional scattering channels with $\nu > 2$, which are not included in the theory for ω_h [45]. We note that two degenerate minima appear in the lowest band for $\alpha > 0.7$, giving rise to the small kinks in the expected loss rates in Fig. 2(e).
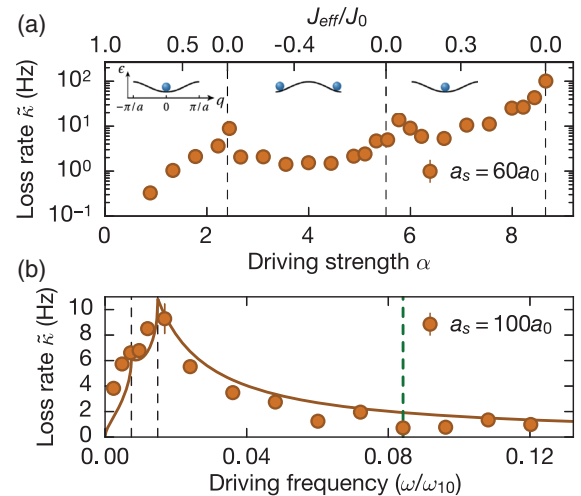
FIG. 4. Loss rates for large driving strengths and small frequencies. (a) When scanning the driving strength α at frequency ω_l, we observe peaks in the loss rate whenever the effective tunneling $J_{\rm eff} = J_0 \cdot \mathcal{J}_0(\alpha)$ goes through zero (dashed lines). The insets sketch the lowest band for positive and negative tunneling. (b) For a fixed driving strength $\alpha = 1.1$, we observe a peak in the loss rate for driving frequencies close to the bandwidth of the lowest band. The solid line shows the theory scaled by $f\beta\hbar\omega$ with a temperature of 15 nK (see the text). The dashed black lines indicate one (two) times the effective bandwidth, below which the number of accessible states for two- (single-) photon scattering becomes reduced [45]. The dashed green line marks the frequency ω_l. Error bars indicate fit errors.

We also measured the loss rates for large driving amplitudes and low-frequency ω_l; see Fig. 4(a). We can observe clear maxima in the loss rate whenever the effective tunneling matrix element J_{eff} is close to zero and attribute them to zero-photon scattering in the effectively flat band. Interestingly, the loss rate decreases again once the sign of the effective tunneling matrix element J_{eff} changes. Figure 4(b) shows the loss rate for various frequencies close to the bandwidth. Since there are fewer modes available for frequencies below the bandwidth of the lowest band, a clear decrease in the loss rates can be observed [45].

Conclusion and outlook.—We have measured the loss rates of an interacting BEC in a driven one-dimensional optical lattice. They approximately scale with the interaction as $a_s^{7/5}$, in agreement with a theoretical description based on a Thomas-Fermi approximation and Fermi's golden rule. For large driving frequencies, scattered particles can leave the trap and carry away the absorbed energy quanta $\hbar\omega_h$. This mechanism of continuous Floquet evaporative cooling can act as a powerful general strategy to reduce heating rates in Floquet engineered quantum gases. Furthermore, the two-particle scattering processes considered here rely on exciting transverse motion and might therefore be absent in a three-dimensional lattice. Another intriguing possibility is the use of nonergodic or many-body localized systems, where the dynamics can be immune to these heating processes.

[1] A. Zenesini, H. Lignier, D. Ciampini, O. Morsch, and E. Arimondo, Coherent Control of Dressed Matter Waves, Phys. Rev. Lett. **102**, 100403 (2009).

[2] J. Struck, C. Ölschläger, R. Le Targat, P. Soltan-Panahi, A. Eckardt, M. Lewenstein, P. Windpassinger, and K. Sengstock, Quantum simulation of frustrated classical magnetism in triangular optical lattices, Science **333**, 996 (2011).

[3] J. Struck, C. Ölschläger, M. Weinberg, P. Hauke, J. Simonet, A. Eckardt, M. Lewenstein, K. Sengstock, and P. Windpassinger, Tunable Gauge Potential for Neutral and Spinless Particles in Driven Optical Lattices, Phys. Rev. Lett. **108**, 225304 (2012).

[4] C. V. Parker, L.-C. Ha, and C. Chin, Direct observation of effective ferromagnetic domains of cold atoms in a shaken optical lattice, Nat. Phys. **9**, 769 (2013).

[5] G. Jotzu, M. Messer, R. Desbuquois, M. Lebrat, T. Uehlinger, D. Greif, and T. Esslinger, Experimental realization of the topological Haldane model with ultracold fermions, Nature (London) **515**, 237 (2014).

[6] L.-C. Ha, L. W. Clark, C. V. Parker, B. M. Anderson, and C. Chin, Roton-Maxon Excitation Spectrum of Bose Condensates in a Shaken Optical Lattice, Phys. Rev. Lett. **114**, 055301 (2015).

[7] F. Meinert, M. J. Mark, K. Lauber, A. J. Daley, and H.-C. Nägerl, Floquet Engineering of Correlated Tunneling in the Bose-Hubbard Model with Ultracold Atoms, Phys. Rev. Lett. **116**, 205301 (2016).

[8] M. E. Tai, A. Lukin, M. Rispoli, R. Schittko, T. Menke, D. Borgnia, P. M. Preiss, F. Grusdt, A. M. Kaufman, and M. Greiner, Microscopy of the interacting Harper-Hofstadter model in the few-body limit, Nature (London) **546**, 519 (2017).

[9] M. Aidelsburger, M. Atala, M. Lohse, J. T. Barreiro, B. Paredes, and I. Bloch, Realization of the Hofstadter Hamiltonian with Ultracold Atoms in Optical Lattices, Phys. Rev. Lett. **111**, 185301 (2013).

[10] M. Aidelsburger, M. Lohse, C. Schweizer, M. Atala, J. T. Barreiro, S. Nascimbene, N. R. Cooper, I. Bloch, and N. Goldman, Measuring the Chern number of Hofstadter bands with ultracold bosonic atoms, Nat. Phys. **11**, 162 (2015).

[11] C. J. Kennedy, W. C. Burton, W. C. Chung, and W. Ketterle, Observation of Bose-Einstein condensation in a strong synthetic magnetic field, Nat. Phys. **11**, 859 (2015).

[12] J. Struck, M. Weinberg, C. Ölschläger, P. Windpassinger, J. Simonet, K. Sengstock, R. Hoppner, P. Hauke, A. Eckardt, M. Lewenstein, and L. Mathey, Engineering Ising-XY spin-models in a triangular lattice using tunable artificial gauge fields, Nat. Phys. **9**, 738 (2013).

[13] A. Eckardt, Colloquium: Atomic quantum gases in periodically driven optical lattices, Rev. Mod. Phys. **89**, 011004 (2017).

[14] T. Oka and H. Aoki, Photovoltaic Hall effect in graphene, Phys. Rev. B **79**, 081406 (2009).

[15] T. Kitagawa, T. Oka, A. Brataas, L. Fu, and E. Demler, Transport properties of nonequilibrium systems under the application of light: Photoinduced quantum Hall insulators without Landau levels, Phys. Rev. B **84**, 235108 (2011).

[16] G. Usaj, P. M. Perez-Piskunow, L. E. F. Foa Torres, and C. A. Balseiro, Irradiated graphene as a tunable Floquet topological insulator, Phys. Rev. B **90**, 115423 (2014).

[17] D. Fausti, R. I. Tobey, N. Dean, S. Kaiser, A. Dienst, M. C. Hoffmann, S. Pyon, T. Takayama, H. Takagi, and A. Cavalleri, Light-induced superconductivity in a stripe-ordered cuprate, Science **331**, 189 (2011).

[18] R. Matsunaga, N. Tsuji, H. Fujita, A. Sugioka, K. Makise, Y. Uzawa, H. Terai, Z. Wang, H. Aoki, and R. Shimano, Light-induced collective pseudospin precession resonating with Higgs mode in a superconductor, Science **345**, 1145 (2014).

[19] M. Mitrano, A. Cantaluppi, D. Nicoletti, S. Kaiser, A. Perucchi, S. Lupi, P. Di Pietro, D. Pontiroli, M. Ricc, S. R. Clark, D. Jaksch, and A. Cavalleri, Possible light-induced superconductivity in K3C60 at high temperature, Nature (London) **530**, 461 (2016).

[20] V. Khemani, A. Lazarides, R. Moessner, and S. L. Sondhi, Phase Structure of Driven Quantum Systems, Phys. Rev. Lett. **116**, 250401 (2016).

[21] C. W. von Keyserlingk, V. Khemani, and S. L. Sondhi, Absolute stability and spatiotemporal long-range order in Floquet systems, Phys. Rev. B **94**, 085112 (2016).

[22] D. V. Else, B. Bauer, and C. Nayak, Floquet Time Crystals, Phys. Rev. Lett. **117**, 090402 (2016).

[23] N. Y. Yao, A. C. Potter, I.-D. Potirniche, and A. Vishwanath, Discrete Time Crystals: Rigidity, Criticality, and Realizations, Phys. Rev. Lett. **118**, 030401 (2017).

[24] S. Choi, J. Choi, R. Landig, G. Kucsko, H. Zhou, J. Isoya, F. Jelezko, S. Onoda, H. Sumiya, V. Khemani, C. von Keyserlingk, N. Y. Yao, E. Demler, and M. D. Lukin, Observation of discrete time-crystalline order in a disordered dipolar many-body system, Nature (London) **543**, 221 (2017).

[25] J. Zhang, P. W. Hess, A. Kyprianidis, P. Becker, A. Lee, J. Smith, G. Pagano, I.-D. Potirniche, A. C. Potter, A. Vishwanath, N. Y. Yao, and C. Monroe, Observation of a discrete time crystal, Nature (London) **543**, 217 (2017).

[26] A. Lazarides, A. Das, and R. Moessner, Equilibrium states of generic quantum systems subject to periodic driving, Phys. Rev. E **90**, 012110 (2014).

[27] L. D'Alessio and M. Rigol, Long-Time Behavior of Isolated Periodically Driven Interacting Lattice Systems, Phys. Rev. X **4**, 041048 (2014).

[28] A. Eckardt and M. Holthaus, Avoided Level Crossing Spectroscopy with Dressed Matter Waves, Phys. Rev. Lett. **101**, 245302 (2008).

[29] D. Poletti and C. Kollath, Slow quench dynamics of periodically driven quantum gases, Phys. Rev. A **84**, 013615 (2011).

[30] S. Choudhury and E. J. Mueller, Stability of a Floquet Bose-Einstein condensate in a one-dimensional optical lattice, Phys. Rev. A **90**, 013621 (2014).

[31] S. Choudhury and E. J. Mueller, Transverse collisional instabilities of a Bose-Einstein condensate in a driven one-dimensional lattice, Phys. Rev. A **91**, 023624 (2015).

[32] S. Choudhury and E. J. Mueller, Stability of a Bose-Einstein condensate in a driven optical lattice: Crossover between weak and tight transverse confinement, Phys. Rev. A **92**, 063639 (2015).

[33] A. Eckardt and E. Anisimovas, High-frequency approximation for periodically driven quantum systems from a Floquet-space perspective, New J. Phys. **17**, 093039 (2015).

[34] T. Bilitewski and N. R. Cooper, Scattering theory for Floquet-Bloch states, Phys. Rev. A **91**, 033601 (2015).

[35] T. Bilitewski and N. R. Cooper, Population dynamics in a Floquet realization of the Harper-Hofstadter Hamiltonian, Phys. Rev. A **91**, 063611 (2015).

[36] M. Bukov, S. Gopalakrishnan, M. Knap, and E. Demler, Prethermal Floquet Steady States and Instabilities in the Periodically Driven, Weakly Interacting Bose-Hubbard Model, Phys. Rev. Lett. **115**, 205301 (2015).

[37] C. Sträter and A. Eckardt, Interband heating processes in a periodically driven optical lattice, Z. Naturforsch. A **71**, 909 (2016).

[38] E. Canovi, M. Kollar, and M. Eckstein, Stroboscopic prethermalization in weakly interacting periodically driven systems, Phys. Rev. E **93**, 012130 (2016).

[39] T. Kuwahara, T. Mori, and K. Saito, Floquet-Magnus theory and generic transient dynamics in periodically driven many-body quantum systems, Ann. Phys. (Amsterdam) **367**, 96 (2016).

[40] P. Bordia, H. Lüschen, U. Schneider, M. Knap, and I. Bloch, Periodically driving a many-body localized quantum system, Nat. Phys. **13**, 460 (2017).

[41] M. Weinberg, C. Ölschläger, C. Sträter, S. Prelle, A. Eckardt, K. Sengstock, and J. Simonet, Multiphoton interband excitations of quantum gases in driven optical lattices, Phys. Rev. A **92**, 043621 (2015).

[42] D. H. Dunlap and V. M. Kenkre, Dynamic localization of a charged particle moving under the influence of an electric field, Phys. Rev. B **34**, 3625 (1986).

[43] C. Sias, H. Lignier, Y. P. Singh, A. Zenesini, D. Ciampini, O. Morsch, and E. Arimondo, Observation of Photon-Assisted Tunneling in Optical Lattices, Phys. Rev. Lett. **100**, 040404 (2008).

[44] C. D'Errico, M. Zaccanti, M. Fattori, G. Roati, M. Inguscio, G. Modugno, and A. Simoni, Feshbach resonances in ultracold 39 K, New J. Phys. **9**, 223 (2007).

[45] See Supplemental Material at http://link.aps.org/supplemental/10.1103/PhysRevLett.119.200402 for experimental methods, the theoretical estimation of condensate depletion, and Refs. [4,28,30,31,33,33–35,37,41,46–51].

[46] L. De Sarlo, P. Maioli, G. Barontini, J. Catani, F. Minardi, and M. Inguscio, Collisional properties of sympathetically cooled ^{39}K, Phys. Rev. A **75**, 022715 (2007).

[47] F. Ferlaino, C. D'Errico, G. Roati, M. Zaccanti, M. Inguscio, G. Modugno, and A. Simoni, Feshbach spectroscopy of a K-Rb atomic mixture, Phys. Rev. A **73**, 040702 (2006).

[48] V. Bagnato, D. E. Pritchard, and D. Kleppner, Bose-Einstein condensation in an external potential, Phys. Rev. A **35**, 4354 (1987).

[49] M. Genske and A. Rosch, Floquet-Boltzmann equation for periodically driven Fermi systems, Phys. Rev. A **92**, 062108 (2015).

[50] H. Sambe, Steady states and quasienergies of a quantum-mechanical system in an oscillating field, Phys. Rev. A **7**, 2203 (1973).

[51] N. Goldman and J. Dalibard, Periodically Driven Quantum Systems: Effective Hamiltonians and Engineered Gauge Fields, Phys. Rev. X **4**, 031027 (2014).

[52] H. Lignier, C. Sias, D. Ciampini, Y. Singh, A. Zenesini, O. Morsch, and E. Arimondo, Dynamical Control of Matter-Wave Tunneling in Periodic Potentials, Phys. Rev. Lett. **99**, 220403 (2007).